PHYSICAL REVIEW A **88**, 043803 (2013)

Measurement of the Gouy phase anomaly for electron waves

T. C. Petersen,[1,2,*] D. M. Paganin,[1] M. Weyland,[2,3] T. P. Simula,[1] S. A. Eastwood,[1] and M. J. Morgan[1]

[1]*School of Physics, Monash University, Victoria 3800, Australia*

[2]*Monash Centre for Electron Microscopy, Monash University, Victoria 3800, Australia*

[3]*Department of Materials Engineering, Monash University, Victoria 3800, Australia*

(Received 24 May 2013; published 4 October 2013)

We measure the Gouy phase anomaly for matter waves using in-line holography to retrieve the full complex field of an astigmatic electron wave function. Sequential phase shifts of $\pi/2$ rad are observed for electron trajectories along the optic axis that pass through each line-focus caustic of subnanometer transverse width. Our observations demonstrate that anomalous phase shifts of matter waves in the vicinity of caustics can be robustly measured using phase retrieval, extending the current scope of singular electron optics.

DOI: 10.1103/PhysRevA.88.043803 PACS number(s): 42.25.−p, 41.85.−p, 42.30.Rx, 42.50.Xa

I. INTRODUCTION

The Gouy phase anomaly [1], which describes the additional phase shift accumulated by a wave packet upon focusing, has been of fundamental interest in light optics for more than a century, and the diverse literature on this phenomenon continues to grow. Understanding, measuring, and ultimately exploiting the Gouy phase in a variety of experimental contexts is crucial for the development of particular optical technologies. For example, the rotation of the Poynting vector in Laguerre-Gauss beams is proportional to the Gouy phase [2]. Applications that exploit the phase anomaly include visible-wavelength super-resolution [3], sub-wavelength terahertz (THz) imaging [4], ultrashort laser pulses [5], single nanoparticle interferometry [6], and astigmatic mode conversion [7]. Use of the Gouy phase in this latter situation has been demonstrated for vortical electron beams [8]. In light optics, the rotation of topological defects in Laguerre-Gauss beams [9] has been used as a means to study Gouy phase effects. Such rotations were recently measured and were demonstrated for matter waves in a transmission electron microscope (TEM) [10].

Gouy's original observations were made using mirrors and white-light interferometry [1,11]. Visible-light lasers have since been used to measure the effect [12]. Measurements of the Gouy phase for cylindrically focused waves were reported in visible-light optics [13] where the anomaly was generalized for astigmatic wave fields [14]. Specifically, Visser and Wolf [14] derived the following expression for the on-axis Gouy phase anomaly $\delta(u)$ for a scalar wave diffracted from an aperture of size a, focused by an astigmatic lens of focal length f with coefficient of astigmatism A_0,

$$\delta(u) = \arg\left[\int_0^1 e^{i[(kA_0-u)\rho^2/2]}\rho J_0(kA_0\rho^2/2)d\rho\right] - \frac{\pi}{2}, \tag{1}$$

where J_0 is a zeroth-order Bessel function of the first kind and the integration variable ρ is dimensionless. The parameter u is proportional to the distance z along the optic axis according to $u = 2\pi(a/f)^2 z/\lambda$, where λ is the wavelength and k is the wave number. Equation (1) describes two sequential Gouy phase shifts of $\pi/2$ rad along the optic axis, associated with a pair of mutually orthogonal line foci, separated by $\Delta u = 2kA_0$ (see Fig. 1).

Refracting objects can act as natural lenses and inherently can give rise to Gouy phase shifts. For example, near the focal point of a light-scattering microsphere, the phase anomaly has been retrieved using a modified Hartman wave-front sensor [15]. The Gouy phase has also been measured in other contexts, such as the local expansion of adjacent intensity minima in standing microwaves [16], time-resolved THz pulses [17], and the cylindrical focusing of phonon-polariton wave packets in Raman scattering [18].

Recently, experiments were proposed for measuring the Gouy phase in matter waves, such as coherent atomic beams, using cylindrical focusing of Rydberg atoms [19]. Inspired by this proposal, we have measured the Gouy phase for astigmatic electron matter waves using phase retrieval [20,21]. Aberration correction lenses in a TEM were used to induce astigmatic pairs of line foci with transverse cross sections narrower than 1 nm, separated by more than 1 μm along the longitudinal optic axis. Through-focal series of images were used to retrieve the wave-function phase; the Gouy anomaly through each line focus was measured by propagating the retrieved electron wave function.

II. EXPERIMENT

Figure 1 shows a schematic of the experiment where electron matter waves diffracted by a circular aperture are focused by an astigmatic lens, which produces a caustic volume containing a pair of mutually orthogonal line foci at different points along the optic axis in the vicinity of the backfocal plane of the aberrated lens.

With a small 10-μm condenser aperture, a thin disordered carbon specimen was used to correct the aberrations in the imaging lens on a Titan^3 80-300 (FEI) aberration-corrected (CEOS GmbH) TEM, operating at 300 kV. Without fully correcting aberrations in the probe-forming lenses, the condenser system was configured to produce a small yet parallel probe, and the first condenser lens was adjusted to about half the maximum nominal setting. Airy rings were observed upon convergence of the electron probe in the imaging plane after which the probe-corrector stigmator coils were then grossly

*Corresponding author: timothy.petersen@monash.edu

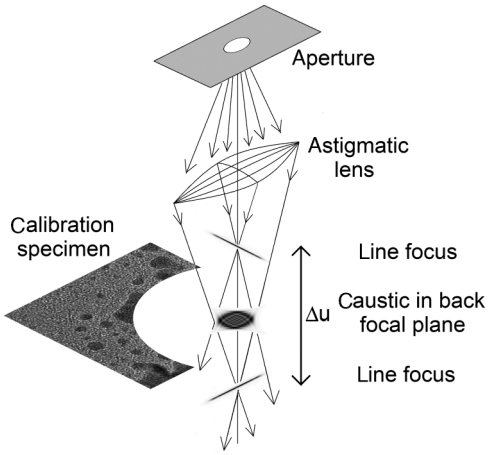

FIG. 1. Schematic of electron matter waves diffracted by a circular aperture and focused by a lens with astigmatism. The Gouy phase anomaly describes the variation in the electron wave phase along the longitudinal (vertical) optic axis, through the transverse center of the aberrated focal volume as compared to the linear variation of phase predicted by geometric optics. A thin specimen is used to correct imaging lens aberrations with a parallel probe, prior to the imposition of astigmatism in the illumination and focusing of the probe in the specimen plane. The parameter u is proportional to the distance along the optic axis as described in the paragraph containing Eq. (1).

excited to produce an astigmatic line focus of subnanometer width. Defocusing of the imaging objective lens revealed another mutually orthogonal line focus about 1.5 μm farther along the optic axis. A micron-sized hole in the specimen was found so that images of electron probe cross sections could be observed in the absence of scattering. Using 100 s acquisition times, a focal series of 12 images was collected at points along the optic axis between the two line foci, using nominal defocus increments of 60 nm.

The electron phase was retrieved using the Gerchberg-Saxton-Misell algorithm [20,21], which propagates a paraxial wave between focal planes and replaces wave intensities with those measured in experiment. Starting with an initial phase estimate, iterations of this process can retrieve the wave function with transverse probability distributions that are consistent with experimental observations. Although alternative approaches exist, this algorithm was employed to reliably handle intensity zeros surrounding caustic cross sections as well as possible phase vortices [22,23], which arise in the focal volumes of lenses with aberrations [24,25]. To increase the signal-to-noise ratio, all images were down-sampled from 2048×2048 pixels to 256×256 pixels. For improved robustness to noise, propagated waves were averaged in a fixed plane with each iteration using the approach of Allen *et al.* [23], but excluding the effects of partial coherence. Despite these measures and the long exposure times used to acquire the experimental intensities, the propagated intensities failed to converge towards experiment and the phase-retrieval algorithm stagnated. Some features, such as the caustic shape and blurred line foci, were retrieved; yet after thousands of iterations, the consistency of the wave function intensities with experiment was not satisfactory, even on a qualitative level. To deal with this, we approximated the caustic using a diffraction integral to compute the astigmatic wave function, which was then used to seed the initial phase in the retrieval iterations. Furthermore, the retrieval algorithm was modified to exclude the fitting of intensities far from the caustic where the experimental data contained only noise and were devoid of phase information. This was achieved in a systematic manner by iteratively replacing only those pixels where the experimental intensity was above one standard deviation of the intensity, measured in a region far from the caustic. Satisfactory convergence of propagated intensities towards the experimental input was then achieved after 10^3 iterations. To improve the spatial resolution of diffraction detail within the caustic, the retrieved wave function was then resampled to 1024×1024 pixels and was used to seed a further 10^3 iterations with the experimental data down-sampled to the same number of pixels.

III. ANALYSIS

In principle, any in-line holographic method can be used to reconstruct a desired monochromatic scalar wave function, provided that the solution reproduces the experimental data when propagated between focal planes. Allen *et al.* [23] define a sum-squared error (SSE) to characterize the convergence for iterative phase retrieval, which has the form $\mathrm{SSE}_j = \Sigma\Sigma(\sqrt{I_{\mathrm{exp}}} - \sqrt{I_{\mathrm{rec}}})^2/\Sigma\Sigma I_{\mathrm{exp}}$, where the double sums are over all pixels in the jth experimental intensity I_{exp} and reconstructed intensity I_{rec}. The average of SSE_j over all N images in the focal series defines an averaged sum-square error: $\mathrm{SSE}_{\mathrm{av}} = \Sigma \mathrm{SSE}_j/N$. Over the entire field of view for all 12 images in the focal series, the caustic reconstruction converged to $\mathrm{SSE}_{\mathrm{av}} = 5.6 \times 10^{-2}$. For all pixels with intensity above the threshold used for iterative replacement, the error metric was measured to be $\mathrm{SSE}_{\mathrm{av}} = 1.4 \times 10^{-2}$.

Figure 2 shows the phase-retrieval results for the astigmatic caustic. Figure 2(a) shows the retrieved phase of the propagated wave function at a focal distance in-between the two line

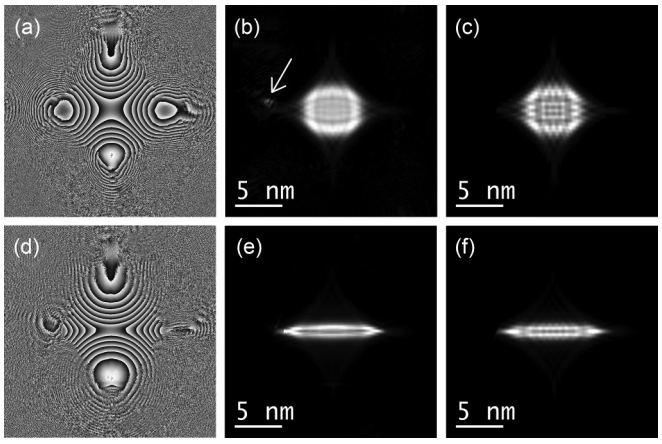

FIG. 2. (a) Retrieved electron phase map at a focal distance in-between the two astigmatic focal lines. (b) Corresponding propagated intensity. (c) Experimental intensity distribution at the same focal distance. (d) Retrieved electron phase map near one of the astigmatic focal lines. (e) Corresponding propagated intensity. (f) Experimental intensity distribution at the same focal distance. The arrow in (b) highlights an outlying discrepancy in the retrieved probability density, discussed in the main text.

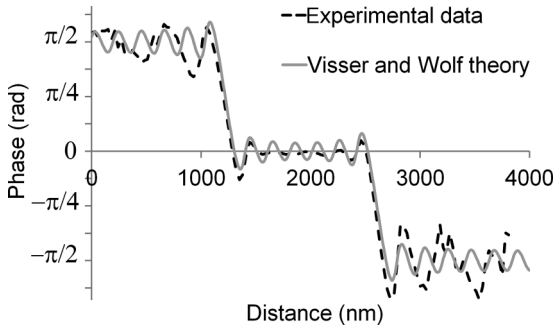

FIG. 3. Experimentally retrieved on-axis phase (dashed curve) for a focused astigmatic matter-wave field compared with the Gouy anomaly theory predicted by Visser and Wolf [14]. Two sequential phase shifts of $\pi/2$ rad occur at each line focus due to the Gouy anomaly. Parameters required for the theory given by Eq. (1) were measured from the experimentally retrieved intensity distributions alone.

foci with the corresponding retrieved intensity in Fig. 2(b), which compares favorably with the experimental data in Fig. 2(c). Figure 2(d) shows the retrieved phase near one of the line foci with the associated retrieved intensity in Fig. 2(e) compared to the experimental data in Fig. 2(f). Close inspection of Fig. 2(f) indicates that the left cusp is clipped since this region was outside the field of view of the CCD used to capture the unprocessed experimental data. This explains the outlying discrepancy labeled in Fig. 2(b), which arose because the intensity in this region was unconstrained and the clipping of the experimental data is an unphysical artifact. Figures 2(e) and 2(f) also show good agreement, thereby demonstrating satisfactory convergence of the iterative phase-retrieval algorithm, which is consistent with the small value of $\mathrm{SSE}_{\mathrm{av}}$.

Using the retrieved wave function, the centers of the phase maps were tracked by propagating the electron wave in steps of 30 nm along the optic axis. The positions of the sharp line foci in the transverse intensity distributions were used to accurately determine the optic axis position, along which the retrieved on-axis phase was then plotted, as shown by the dashed profile in Fig. 3. The solid-line profile in Fig. 3 was calculated from Eq. (1). Apart from the electron wavelength, three additional parameters were required for the computation, namely, the effective aperture size to focal length ratio a/f, the coefficient of astigmatism A_0, and the position of the line foci. All of these parameters were robustly determined from the intensities of the experimentally retrieved wave function by computing the Heisenberg uncertainties $\Delta x(z)$ and $\Delta y(z)$. Away from the line foci, $\Delta x(z)$ and $\Delta y(z)$ behave asymptotically as $T|z|$, where T is a constant representing the gradient of the uncertainty as a function of the distance z. Each measured value of T was averaged to determine A_0 using Eq. (1) with $a/f \cong 2T$ [14]. Both phase profiles contain an arbitrary vertical offset, which we have systematically chosen so that the on-axis variations approach zero in-between the two line foci.

The experimental on-axis phase profile in Fig. 3 follows the theory of Visser and Wolf [14] closely; in particular, the slopes and horizontal positions of the rapid phase variations near each line focus match. Some differences are evident between the undulations in Fig. 3, which are sensitive to the effects of diffraction. These discrepancies could be ascribed to systematic errors in the phase retrieval. However, we expect differences on account of the fact that large excitation of the TEM stigmator coils does not produce pure twofold astigmatism but, rather, an astigmatic beam with a pair of line foci, which is also perturbed by coma and higher-order aberrations.

In addition to the scalar diffraction theory of focused paraxial waves, a variety of interpretations exist for the Gouy anomaly. One persistent theme is the idea that the Gouy effect arises from fluctuations in the transverse momentum, induced by variations in the uncertainty of the beam at different focal points along the optic axis [26–28]. For Gaussian beams, the variation in the standard deviation is characterized by the evolution of the beam waist, and the transverse intensity distribution maintains the same shape at different points along the optic axis [11]. Accordingly, the Gouy phase evolves along the optic axis, varying most rapidly near the focus and more abruptly for smaller beam waists. Borghi *et al.* [29] have theoretically demonstrated a "universal form" of this Gouy phase variation for a wide class of such shape-invariant beams. The caustic shapes and standard deviations of other beams, such as those formed by astigmatic lenses, are not shape invariant and are nontrivial with interference phenomena more readily described by catastrophe optics [30–32]. We performed another experiment to demonstrate the three-dimensional nature of this standard deviation, organized by the diffraction detail within an astigmatic volume. Similar illumination conditions were chosen, with the exception of the field-emission gun lens, the strength of which was halved, thereby increasing the probe intensity to reduce the Poisson noise in recorded images. Thirty-two images were then acquired using 100-s exposures and nominal defocus increments of 80 nm. These images were stacked to create a tomogram of the matter-wave probability density. Figure 4 shows a false-color isosurface of

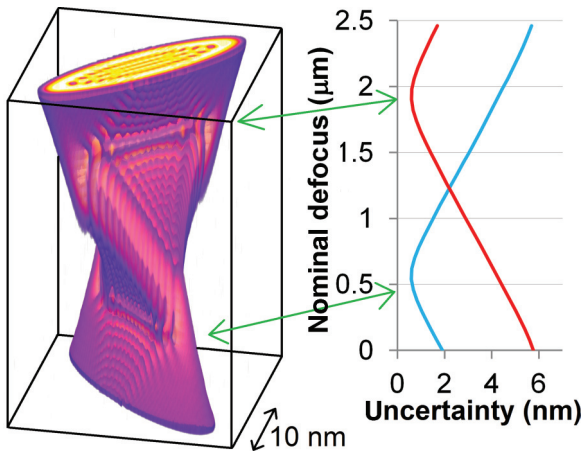

FIG. 4. (Color) Electron probability density measured from a through-focus series of 32 images, which were stacked along the vertical direction and were interpolated. The uncertainties along two transverse directions, orthogonal to each line focus, were calculated from each image. The paraxial electron wave evolves slowly along the optic axis as evidenced by the 10-nm transverse scale bar, which is to be contrasted with the micron-scale focal range along the vertical axis.

the tomogram, which was rendered using the VOLUME VIEWER plug-in for IMAGEJ [33,34]. The accompanying Heisenberg uncertainties were measured along directions orthogonal to the line foci and fall to a minimum at each line focus. These plots and other image-processing operations were performed using the scientific data analysis package DIFFTOOLS [35].

Diffraction effects, due to the finite electron wavelength and the uncertainty principle, prevent the uncertainties from reaching zero in Fig. 4 where the Gouy anomaly varies most rapidly. The entire tomogram of the electron probability density can be viewed as a richly detailed three-dimensional in-line hologram. Several transverse sections of such a volume, which encode the holographic information, enabled the complex field of the matter wave to be retrieved to yield the Gouy anomalies shown in Fig. 3.

IV. CONCLUSION

To summarize, we have measured the Gouy phase anomaly for astigmatic matter waves using electron wave-function phases inferred from experimental intensities. Successive Gouy phase shifts of $\pi/2$ rad were observed for fast electrons traveling along the optic axis, passing through two subnanometer lines of focus. These longitudinal phase variations were compared with wave optics theory, and consistency with experiment was demonstrated. With singular electron optics in its infancy, opportunities exist to extend these findings and to explore quantized phase changes of matter waves in more general settings, such as discrete phase changes for rays that touch caustics, which are characterized by Maslov indices [36,37].

ACKNOWLEDGMENTS

S. Kennedy and D. Jesson from the Monash University School of Physics are thanked for their useful input and stimulation of ideas. The authors acknowledge use of the facilities within the Monash Centre for Electron Microscopy. This research used equipment funded by the Australian Research Council Grant No. LE0454166. Funding from the Australian Research Council Discovery Project Grant No. DP1092745 is also gratefully acknowledged. T. C. Petersen is grateful for financial support from J. Etheridge of the Monash Centre for Electron Microscopy.

[1] L. G. Gouy, Ann. Chim. Phys. **24**, 145 (1891).
[2] M. J. Padgett and L. Allen, Opt. Commun. **121**, 36 (1995).
[3] A. Whiting, A. Abouraddy, B. Saleh, M. Teich, and J. Fourkas, Opt. Express **11**, 1714 (2003).
[4] M. Yi, K. Lee, J. D. Song, and J. Ahn, Appl. Phys. Lett. **100**, 161110 (2012).
[5] F. Lindner, G. G. Paulus, H. Walther, A. Baltuška, E. Goulielmakis, M. Lezius, and F. Krausz, Phys. Rev. Lett. **92**, 113001 (2004).
[6] J. Hwang and W. E. Moerner, Opt. Commun. **280**, 487 (2007).
[7] M. W. Beijersbergen, L. Allen, H. Vanderveen, and J. P. Woerdman, Opt. Commun. **96**, 123 (1993).
[8] P. Schattschneider, M. Stöger-Pollach, and J. Verbeeck, Phys. Rev. Lett. **109**, 084801 (2012).
[9] J. Hamazaki, Y. Mineta, K. Oka, and R. Morita, Opt. Express **14**, 8382 (2006).
[10] G. Guzzinati, P. Schattschneider, K. Y. Bliokh, F. Nori, and J. Verbeeck, Phys. Rev. Lett. **110**, 093601 (2013).
[11] A. E. Siegman, *Lasers* (University Science Books, Saulsalito, CA, 1986).
[12] H. C. Kandpal, S. Raman, and R. Mehrotra, Opt. Lasers Eng. **45**, 249 (2007).
[13] J. P. Rolland, K. P. Thompson, K. S. Lee, J. Tamkin, T. Schmid, and E. Wolf, Appl. Opt. **51**, 2902 (2012).
[14] T. D. Visser and E. Wolf, Opt. Commun. **283**, 3371 (2010).
[15] P. Bon, B. Rolly, N. Bonod, J. Wenger, B. Stout, S. Monneret, and H. Rigneault, Opt. Lett. **37**, 3531 (2012).
[16] C. R. Carpenter, Am. J. Phys. **27**, 98 (1959).
[17] A. B. Ruffin, J. V. Rudd, J. F. Whitaker, S. Feng, and H. G. Winful, Phys. Rev. Lett. **83**, 3410 (1999).
[18] T. Feurer, N. S. Stoyanov, D. W. Ward, and K. A. Nelson, Phys. Rev. Lett. **88**, 257402 (2002).
[19] I. G. da Paz, P. L. Saldanha, M. C. Nemes, and J. G. P. de Faria, New J. Phys. **13**, 125005 (2011).
[20] R. W. Gerchberg and W. O. Saxton, Optik (Jena) **35**, 237 (1972).
[21] D. L. Misell, J. Phys. D: Appl. Phys. **6**, 2200 (1973).
[22] L. J. Allen, H. M. L. Faulkner, K. A. Nugent, M. P. Oxley, and D. Paganin, Phys. Rev. E **63**, 037602 (2001).
[23] L. J. Allen, W. McBride, N. L. O'Leary, and M. P. Oxley, Ultramicroscopy **100**, 91 (2004).
[24] A. Boivin, J. Dow, and E. Wolf, J. Opt. Soc. Am. **57**, 1171 (1967).
[25] K. M. Pavlov, D. M. Paganin, D. J. Vine, J. A. Schmalz, Y. Suzuki, K. Uesugi, A. Takeuchi, N. Yagi, A. Kharchenko, G. Blaj, J. Jakubek, M. Altissimo, and J. N. Clark, Phys. Rev. A **83**, 013813 (2011).
[26] R. W. Boyd, J. Opt. Soc. Am. **70**, 877 (1980).
[27] P. Hariharan and P. A. Robinson, J. Mod. Opt. **43**, 219 (1996).
[28] S. M. Feng and H. G. Winful, Opt. Lett. **26**, 485 (2001).
[29] R. Borghi, M. Santarsiero, and R. Simon, J. Opt. Soc. Am. A **21**, 572 (2004).
[30] T. C. Petersen, M. Weyland, D. M. Paganin, T. P. Simula, S. A. Eastwood, and M. J. Morgan, Phys. Rev. Lett. **110**, 033901 (2013).
[31] M. V. Berry and C. Upstill, in *Progress in Optics*, edited by E. Wolf (Elsevier, New York, 1980), Vol. 18, p. 257.
[32] R. Borghi, Phys. Rev. E **85**, 046704 (2012).
[33] C. A. Schneider, W. S. Rasband, and K. W. Eliceiri, Nat. Methods **9**, 671 (2012).
[34] K. U. Barthel, http://rsbweb.nih.gov/ij/plugins/volume-viewer.html, Berlin, Germany (2012).
[35] D. R. G. Mitchell, Microsc. Res. Tech. **71**, 588 (2008).
[36] J. B. Keller, SIAM Rev. **27**, 485 (1985).
[37] Y. I. Orlov, Radiophys. Quantum Electron. **24**, 154 (1981).